Modeling the dynamics and thermodynamics of volcanic degassing

Article *in* Bulletin of Volcanology · January 1998

DOI: 10.1007/s004450050234

CITATIONS
200

READS
351

2 authors, including:

Stephen Blake
The Open University (UK)
110 PUBLICATIONS **4,746** CITATIONS

SEE PROFILE

Bull Volcanol (1998) 60:307–317

ORIGINAL PAPER

D. S. Stevenson · S. Blake

Modelling the dynamics and thermodynamics of volcanic degassing

Received: 26 September 1997 / Accepted: 11 July 1998

Abstract The rates of passive degassing from volcanoes are investigated by modelling the convective overturn of dense degassed and less dense gas-rich magmas in a vertical conduit linking a shallow degassing zone with a deep magma chamber. Laboratory experiments are used to constrain our theoretical model of the overturn rate and to elaborate on the model of this process presented by Kazahaya et al. (1994). We also introduce the effects of a CO_2–saturated deep chamber and adiabatic cooling of ascending magma. We find that overturn occurs by concentric flow of the magmas along the conduit, although the details of the flow depend on the magmas' viscosity ratio. Where convective overturn limits the supply of gas-rich magma, then the gas emission rate is proportional to the flow rate of the overturning magmas (proportional to the density difference driving convection, the conduit radius to the fourth power, and inversely proportional to the degassed magma viscosity) and the mass fraction of water that is degassed. Efficient degassing enhances the density difference but increases the magma viscosity, and this dampens convection. Two degassing volcanoes were modelled. At Stromboli, assuming a 2 km deep, 30% crystalline basaltic chamber, containing 0.5 wt.% dissolved water, the $\sim 700\ kg\ s^{-1}$ magmatic water flux can be modelled with a 4–10 m radius conduit, degassing 20–100% of the available water and all of the 1 to 4 vol.% CO_2 chamber gas. At Mount St. Helens in June 1980, assuming a 7 km deep, 39% crystalline dacitic chamber, containing 4.6 wt.% dissolved water, the $\sim 500\ kg\ s^{-1}$ magmatic water flux can be modelled with a 22–60 m radius conduit, degassing ~2–90% of the available water and all of the 0.1 to 3 vol.% CO_2 chamber gas. The range of these results is consistent with previous models and observations. Convection driven by degassing provides a plausible mechanism for transferring volatiles from deep magma chambers to the atmosphere, and it can explain the gas fluxes measured at many persistently active volcanoes.

Key words Persistent volcanism · Volcanic gas fluxes · Magma convection · Volcano monitoring

Editorial responsibility: T. Koyaguchi

David S. Stevenson (✉)
Climate Research, Meteorological Office, London Road, Bracknell, RG12 2SZ, UK
Fax: +44 1344 854493
e-mail: dstevenson@meto.gov.uk

Stephen Blake
Department of Earth Sciences, Open University, Milton Keynes, MK7 6AA, UK

Introduction

Persistent volcanism involves prolonged high thermal and volatile fluxes. Examples include persistent lava lakes and open vents (Erebus, Kilauea, Stromboli; Francis et al. 1993), long-lived high-temperature fumarole fields (Momotombo; Menyailov et al. 1986), continuous passive degassing (Etna; Allard et al. 1991), and hot acidic crater lakes fed by a steady supply of heat and magmatic volatiles (Ruapehu, Poás; Hurst et al. 1991; Stevenson 1992; Rowe et al. 1992). The magmatic volatiles are typically dominated by water and SO_2, which are relatively soluble in silicate melts, indicating that the volatiles must have evolved from relatively shallow magma sources. Persistent volcanism lasts for years to millenia and indicates that if gas flux measurements are representative, huge volumes (of the order of cubic kilometers) of magma are processed during such activity (Giggenbach 1987; Francis et al. 1993). However, geophysical studies have not detected very large magma volumes at shallow depths beneath these volcanoes and suggest instead that large magma chambers typically occur at greater depths (>5 km), where most volatiles are undersaturated.

In this paper we investigate the anomalously high volcanic gas fluxes from volcanoes that lack very shallow chambers. We model the transport of magma from

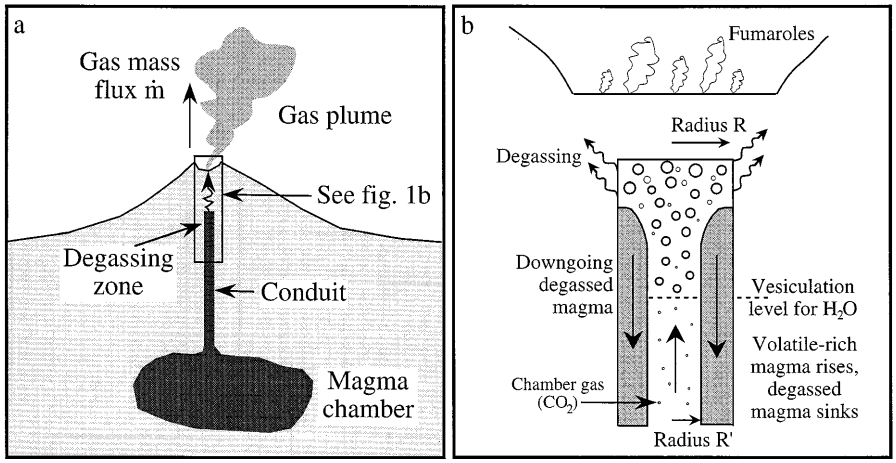

Fig. 1 **a** The modelled magma system. A cylindrical, degassing magma-filled conduit connects a deep chamber to shallow depths. **b** Representation of the degassing zone. The conduit has radius R, and the rising, volatile-rich magma occupies radius R′. Above the vesiculation level, water bubbles nucleate and degassing occurs, leaving behind relatively dense, degassed magma, which sinks, forcing volatile-rich magma upwards

a relatively large, deep chamber to a near-surface zone of gas loss, and the return flow of degassed magma to the source chamber. Kazahaya et al. (1994) have also considered this process and we compare our model to theirs.

Our model involves convection of magma in a conduit connecting a deep chamber to the near-surface (Fig. 1a). The bulk density of the magma in the shallow degassing zone is greater than that of deeper magma as a result of having lost gas bubbles and dissolved volatiles; thus, the degassed magma will sink. Hence, degassing itself provides the driving force for convection. Unlike the model of this process developed by Kazahaya et al. (1994), our model is quantified using measurements from laboratory experiments. Furthermore, we also consider the vesicularity of deep chamber magma as an additional driving force for convection and assess the role of adiabatic cooling in increasing the viscosity of the degassed magma.

We first set up a theoretical model of convective degassing and use it to identify the factors influencing the instantaneous gas flux from a magma body. This model is complemented with the results from simple laboratory experiments, analyzing the behavior of two fluids with different densities and viscosities overturning in a narrow vertical tube. The model is then applied to degassing at Stromboli and following the 18 May 1980 eruption of Mount St. Helens. Stromboli is a classic example of persistent volcanism and has been in a similar state of activity ever since it was first recorded approximately 2000 years ago. Degassing at Mount St. Helens, by contrast, peaked shortly after the climactic eruption and decayed approximately exponentially. Constrained by gas flux and composition data, the model calculates a family of possible solutions for the conduit radius, the amount of water lost from the melt, and the chamber-gas volume fraction.

Modelling convective degassing in a conduit

Model description

The aim of the model described here is to use measured gas fluxes and fumarole compositions to constrain the dimensions and dynamics of degassing volcanic systems. The model is described in Fig. 1a. A cylindrical conduit connects a deep magma chamber to shallow depths. The chamber contains a gas volume fraction of relatively insoluble gases, assumed to be CO_2. Relatively soluble gases (assumed to be H_2O) exsolve from the melt as it depressurizes during ascent in the conduit. The gas mixture subsequently escapes from the magma, supplying a gas flux to the atmosphere. The exact mechanics of bubble escape are unknown, but the important fact is that we know from measurements of gases at the surface that large-scale, rapid magma degassing does occur, often for prolonged periods. The process of gas escape has received a great deal of recent attention through both experimental and theoretical work (e.g., Eichelberger et al. 1986; Jaupart and Vergniolle 1989; Jaupart and Allègre 1991; Proussevitch et al. 1993; Woods and Koyaguchi 1993). The consensus view seems to be that gas can escape relatively easily from low-viscosity basaltic systems but requires the formation and collapse of a foam in more viscous magmas. The rate of degassing at persistently active open vent basaltic volcanoes, such as Stromboli, Masaya, Erebus, and Izu-Oshima, is then likely to be limited by the rate at which gas-rich magma is supplied to the shallow degassing zone (Stevenson 1992; Kazahaya et al. 1994).

Because degassed magma is denser than deeper gas-rich magma, degassing drives convective overturn in the conduit, returning degassed magma to the deep chamber while gas-rich magma rises to replenish the shallow degassing zone. The gas emission rate is assumed to equal the supply rate of gas to the shallow degassing zone. This implies that gas emission is not limited by the gas escape mechanism – a critical assumption that is discussed later. The rate of overturn-

Table 1 Description of symbols and subscripts used

Symbol	Description	Value/Units
c_p	Specific heat capacity at constant pressure	J kg^{-1} K^{-1}
c_v	Specific heat capacity at constant volume	J kg^{-1} K^{-1}
g	Acceleration due to gravity	9.81 m s^{-2}
$\dot{m}$	Mass flux of gas (H_2O, CO_2)	kg s^{-1}
v	Terminal rise velocity of upwelling magma	m s^{-1}
C	Water mass fraction in melt	
ΔC	Difference in C between chamber and degassed melt	
F	Gas mass fraction in chamber	
H_c	Chamber depth	m
$P_{i/f}$	Pressure, initial/final	Pa
Ps	Poiseuille number (equation 1)	
Q	Volumetric magma flow rate	m^3 s^{-1}
R	Radius of conduit	m
R′	Radius of upwelling magma	m
R*	Dimensionless radius of upwelling magma (R′/R)	
$T_{i/f}$	Temperature, initial/final	K
α	Gas volume fraction in chamber	
β	Coefficient of compositional expansion for water in melt	
ϕ	Crystal volume fraction	
γ	Parameter defined by equation (A2)	
μ	Viscosity	Pa s
ρ	Density	kg m^{-3}
$\Delta\rho$	Difference in density driving convection (equations 5 and 6)	kg m^{-3}
τ	Incubation time of convective instability	s
τ^*	Dimensionless incubation time (equation 12)	
Subscripts		
c	Chamber or ascending (ρ, μ, ϕ)	
d	Degassed or descending (ρ, μ, ϕ)	
l	Liquid or melt (ρ, μ)	
m	Magma (ρ, μ)	
0	Anhydrous (ρ_l)	

ing places an upper limit on the rate of gas emission and depends on the density difference between the degassed and gas-rich magmas ($\Delta\rho$) and the viscosities of the ascending magma (μ_c) and descending magma (μ_d). All of the symbols and subscripts used are defined in Table 1.

If the rising chamber magma occupies a radius R′ within the conduit of radius R (Fig. 1b), then, at low Reynolds number, its terminal rise velocity (v) will be parameterized by a Poiseuille number (Ps; c.f. Koyaguchi and Blake 1989):

$$\mathrm{Ps} = \frac{\mathrm{v}\,\mu_d}{\mathrm{g}\,\Delta\rho \mathrm{R}^2} = \mathrm{f}(\mu_d/\mu_c, \mathrm{R}^*), \tag{1}$$

where R* is the dimensionless radius of the rising fluid, given by (R′/R), and g is the acceleration due to gravity. (A later section describes the experimental determination of the relationship between Ps, μ_d/μ_c, and R*, and verifies the assumption of concentric flow.)

The gas flux then depends on the volumetric magma upflow rate (Q):

$$\mathrm{Q} = \pi(\mathrm{R}')^2\mathrm{v} = \pi(\mathrm{R}^*)^2\,\mathrm{Ps}\left(\frac{\mathrm{g}\,\Delta\rho\,\mathrm{R}^4}{\mu_{ld}}\right), \tag{2}$$

and the amount of gas lost. The amount of water lost is the difference between the water content of the chamber melt (C_{lc}) and the degassed melt (C_{ld}):

$$\Delta\mathrm{C} = \mathrm{C}_{lc} - \mathrm{C}_{ld}. \tag{3}$$

ΔC can range between zero (no water degassing) and C_{lc} (complete water degassing), depending on the efficiency of gas loss.

The densities of the degassed melt (ρ_{ld}) and chamber melt (ρ_{lc}) are given by:

$$\rho_{ld} = \rho_{l0}(1 - \beta\mathrm{C}_{ld}) \tag{4a}$$

and

$$\rho_{lc} = \rho_{l0}(1 - \beta\mathrm{C}_{lc}), \tag{4b}$$

where ρ_{l0} is the anhydrous melt density and β is the coefficient of compositional expansion for water. By calculating the densities of hydrous melts as a function of water content, with the partial molar volume of water in silicate melts assumed to be 17 cm^3 mol^{-1} (Lange and Carmichael 1990), β was found to range from 1.17 (for dacite) to 1.55 (for basalt). Melt density increases as dissolved water content decreases. For the simple case of crystal-free magmas, and a non-vesicular magma chamber, the density difference driving convection is:

$$\Delta\rho = \rho_{ld} - \rho_{lc} = \rho_{l0}\beta\Delta\mathrm{C}. \tag{5}$$

More generally, if the deep chamber contains a volume fraction α of highly insoluble gas (CO_2), with gas density ρ_{CO2} at the top of the chamber, and a crystal volume fraction in the chamber ϕ_c with the crystal density as-

sumed to be equal to that of the chamber melt (ρ_{lc}), then the density difference driving convection is:

$$\Delta\rho = \rho_{l0}\beta\Delta C(1-\phi_d) + \alpha(\rho_{lc} - \rho_{CO2}), \quad (6)$$

where $\phi_d = \phi_c / (1-\alpha)$; ϕ_d is the crystal volume fraction in the degassed magma. The first term on the right-hand side represents the contribution due to dehydration of the melt, and the second term represents the contribution due to the vesicularity of the deep magma. The gas density at the top of the chamber is used because we assume that Q is limited by the minimum value of $\Delta\rho$ in the conduit, which occurs where the magma enters the conduit. It has also been assumed that crystallization in the conduit is negligible (see Discussion).

The magma flow rate, Q, also depends on the viscosities of the magmas (Eq. (2)). Viscosity increases as the amount of dissolved water decreases (McBirney and Murase 1984). Removal of 1 wt.% water typically increases melt viscosity by a factor of ~10. Melt viscosities (μ_l) are calculated as a function of composition, temperature, and water content according to Shaw (1972) and are then used to calculate the viscosity of crystal-bearing magma (μ_m; e.g., Tait and Jaupart 1990):

$$\mu_m = \mu_l(1-\phi)^{-2.5}. \quad (7)$$

The amount of water lost by degassing and the rate at which magma overturns in the conduit determine the water mass flux ($\dot{m}_{H2O}$) from the degassing zone:

$$\dot{m}_{H2O} = Q(1-\phi_c-\alpha)\rho_{lc}\,\Delta C. \quad (8)$$

The CO_2 mass flux ($\dot{m}_{CO2}$) is given by:

$$\dot{m}_{CO2} = Q\rho_{CO2}\alpha, \quad (9)$$

where the gas density is calculated at the depth of the top of the chamber. The ratio of the mass fluxes of water and CO_2 is equivalent to the mass ratio of these gases in fumaroles ($[H_2O]/[CO_2]$), a commonly measured quantity, and adds a further constraint to the modelling. Taking the ratio of the fluxes yields:

$$\alpha = \frac{(1-\phi_c)\rho_{lc}\Delta C}{\rho_{lc}\Delta C + \rho_{CO2}\dfrac{[H_2O]}{[CO_2]}}. \quad (10)$$

Hence, for a given fumarole composition, the gas volume fraction in the chamber can be estimated. The main control on α in this equation is the gas density, which is proportional to chamber depth. In general, a higher chamber-gas content increases the density contrast and hence increases gas fluxes. However, another impact of chamber gas on the ascending magma is cooling due to expansion of the gas. This cooling can significantly increase magma viscosity at high chamber-gas contents (e.g., Giberti et al. 1992) and reduce gas fluxes. For most magmas, however, the effect is likely to be minor (see Appendix).

In summary, the model calculates the maximum H_2O and CO_2 fluxes that can be sustained by convective degassing as a function of input values of magma composition (chamber-water content, crystal content, and gas fraction) and temperature, conduit radius, amount of water degassed, and chamber depth. The sensitivity of the calculated gas fluxes to these input variables is investigated. Given a measured gas flux and a fumarole composition, together with other relatively well-constrained input variables, inverse application of the model can be used to estimate poorly constrained variables such as conduit radius and the amount of water degassed.

Before the model can be applied quantitatively, the relationships between the Poiseuille number (Ps), the viscosity ratio (μ_d/μ_c), and the dimensionless radius of the rising fluid (R*) need to be found experimentally.

Laboratory experiments

To test Eq. (1) and to investigate the style of overturn, we conducted several laboratory experiments using miscible fluids of different densities and viscosities and long, narrow glass tubes. The tubes had aspect ratios of approximately 100. Water and solutions of golden syrup and glycerol were the fluids used. Viscosities were measured by the falling-sphere method in a long tube, taking into account wall effects (Clift et al. 1978). Densities were measured by weighing known volumes. Uncertainties of ~20% in measured viscosity values, due to the lack of temperature control in the laboratory, are the major source of error in the experiments. The lower half of the tube was filled with the denser, more viscous fluid (density ρ_d, viscosity μ_d); then the rest of the tube was filled with the less dense, less viscous fluid (ρ_c, μ_c), and the top corked. The tube was then inverted. The interface between the two fluids became unstable after a short incubation period, and the less dense fluid rose up the center of the pipe, rapidly reaching a constant speed, v. Results are summarized in Table 2.

Three different overturn styles were observed: (a) at low viscosity ratios ($\mu_d/\mu_c < \sim 10$), the descending fluid rapidly detached from the wall and descended down the center of the tube, forming an approximate mirror image of the rising fluid (Fig. 2a); (b) at intermediate viscosity ratios ($\sim 10 < \mu_d/\mu_c < \sim 300$), the descending fluid eventually detached from the wall, then split into blobs falling down the center of the tube (Fig. 2b); and (c) at high viscosity ratios ($\mu_d/\mu_c > \sim 300$), the descending fluid remained stuck to the walls (Fig. 2c).

It was not possible to accurately measure the radius of the rising fluid finger in our experiments, because of optical distortion caused by the glass tubing. To estimate radii, four further experiments were conducted, where a long bubble (aspect ratio ~20) of low-viscosity fluid was injected into the base of a vertical, open-ended column of denser, more viscous fluid. By measuring the bubble length and the volumetric displacement of the liquid column when the fluid was injected, the bubble radius (R′) and hence the dimensionless ra-

Table 2 Summary of experimental data and results. Measured viscosities (μ) and densities (ρ) of the rising (subscript c) and descending (subscript d) fluids, pipe radii (R), observed terminal rise velocities (v), calculated Poiseuille numbers (Ps), incubation times (τ), dimensionless incubation times (τ^*), and, for the bubble experiments, inferred bubble radii (R′) and dimensionless bubble radii (R*). Dil = Dilute, V.Dil = Very dilute

Experiment	μ_d/Pa s	μ_c/Pa s	ρ_d/kg m^{-3}	ρ_c/kg m^{-3}	$\Delta\rho$/kg m^{-3}	R/mm	v/10^{-5} m s^{-1}	$\log_{10}(\mu_d/\mu_c)$	Ps	τ/s	τ^*	R′/mm	R*
Overturn													
1. Syrup/dil syrup	102	1.49	1427	1350	77	7.2	2.51	1.84	0.065	440	23.5		
2. Syrup/v.dil syrup	111	0.006	1427	1143	284	4.0	2.61	4.27	0.065	112	11.2		
3. Dil.syrup/glycerol	2.05	1.61	1382	1257	125	4.0	22.0	0.10	0.023	4.4	10.5		
4. Dil.syrup/glycerol	4.37	1.87	1404	1257	147	4.0	17.1	0.37	0.032	10.0	13.2		
5. Glycerol/water	1.87	0.0011	1257	1000	257	4.0	132	3.23	0.061				
6. Syrup/dil syrup	67.2	0.049	1426	1282	144	4.0	2.27	3.14	0.067	354	29.8		
7. Syrup/water	38.1	0.0011	1423	1000	423	7.2	36.8	4.54	0.065				
8. Syrup/water	33.6	0.0011	1423	1000	423	7.2	40.0	4.48	0.062				
9. Syrup/glycerol	54.9	1.87	1425	1257	168	7.2	9.43	1.47	0.061	27	5.8		
10. Dil syrup/glyc	2.24	1.06	1380	1257	123	7.2	99.5	0.32	0.036				
11. Dil syrup/glyc	2.24	1.06	1380	1257	123	4.0	27.3	0.32	0.032				
Bubble													
B2. Syrup/water	161	0.0011	1429	1000	429	7.2	8.97	5.16	0.066			3.8	0.53
B3. Syrup/water	45.2	0.0011	1424	1000	424	7.2	24.6	4.61	0.052			4.6	0.64
B4. Syrup/glyc	47.2	1.05	1424	1257	167	7.2	11.2	1.65	0.062			4.6	0.64
B5. Dilsyrup/glyc	2.24	1.06	1380	1257	123	7.2	84.5	0.32	0.030			4.3	0.60

Fig. 2a–c The three different overturn styles. **a** At low viscosity ratios, the descending fluid detaches from the wall and assumes approximately the same morphology as the rising fluid; **b** at intermediate viscosity ratios, the descending fluid eventually detaches from the walls and splits into individual blobs that descend down the center of the pipe; **c** at high viscosity ratios, the descending fluid sticks to the walls

dius (R*) were calculated (Table 2). Values of R* were approximately constant with values of 0.64–0.53, across a broad range of values of Ps and μ_d/μ_c. These long bubbles were found, within error, to rise with the same velocity as when the same fluids overturned (Fig. 3; Table 2), suggesting that the fluid dynamics are essentially the same, and that $R^* = 0.6$ adequately describes the overturn experiments. This value is not at odds with qualitative observations of the experiments.

For constant R*, Eq. (1) becomes $Ps = f(\mu_d/\mu_c)$, so Poiseuille numbers were plotted against viscosity ratio (Fig. 3). At intermediate to high viscosity ratios, values of Ps averaged ~ 0.064, but smaller values were found for viscosity ratios less than ~ 10. In the following models we use values of Ps as follows:

$$Ps = 0.064 \quad (\mu_d/\mu_c > 12) \tag{11a}$$

$$Ps = 0.020 + 0.041 \log_{10}(\mu_d/\mu_c) \quad (1 < \mu_d/\mu_c < 12). \tag{11b}$$

These experimental results can be compared with the theory of Kazahaya et al. (1994), who solved the equations for flow in a concentric double-walled pipe, with upflow in a central pipe balanced by downflow in an outer annulus. Their solutions indicate that the position of the boundary between upflow and downflow (R*) is a function of the viscosity ratio (μ_d/μ_c; Eq. (13); Kazahaya et al. 1994) and lead to a theoretical relation between Poiseuille number and viscosity ratio plotted in Fig. 3. There is moderate agreement between the theory and experiments at low viscosity ratio, but as the ratio increases, the Kazahaya et al. (1994) theory pre-

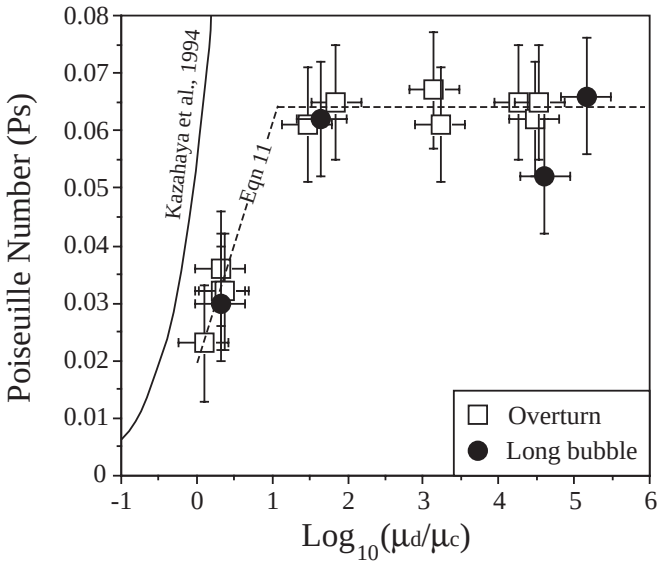

Fig. 3 Plot of Poiseuille number (Eq. (1)) against log viscosity ratio (μ_d/μ_c), for all of the overturn (*squares*) and bubble injection (*circles*) experiments. Ps has an approximately constant value of ~ 0.064 when $\mu_d/\mu_c > \sim 12$, but has lower values at lower viscosity ratios (Eqs. (11a, b)). *Error bars* are estimated from the uncertainty in viscosity measurements. Also shown is the Kazahaya et al. (1994) model of counterflow in a pipe

dicts much higher values for Ps, and much lower values for R^*, than experimentally observed (e.g., $R^* = 0.3$ at $\mu_d/\mu_c = 100$). The reason for this discrepancy is probably Kazahaya et al.'s (1994) incorrect assumption of zero velocity at the interface between the two fluids.

The incubation time (τ), or time intercept on the time-distance graph for the rising fluid finger, is a characteristic feature of the gravitational instability of fluid interfaces (e.g., Lister and Kerr 1989). A dimensionless incubation time may be defined as

$$\tau^* = \frac{\tau g \Delta\rho R}{\mu_{ld}} \qquad (12)$$

and, according to the accuracy of our technique, appears independent of viscosity ratio (Table 2), with a value of ~ 10. Substituting typical values for a large dacite-filled conduit ($R \sim 40$ m) and a small basalt-filled conduit ($R \sim 5$ m) yields incubation times of approximately 1 h and 1 min, respectively. This indicates that once an unstable density gradient is established, the onset of convection is essentially instantaneous.

Application of the model

Here we investigate the influence of four variables upon the water flux from the degassing zone given by Eq. (8): the amount of degassed water (ΔC), conduit radius (R), crystal content of the chamber magma (ϕ_c), and the chamber-gas volume fraction (α). The magnitude of degassing affects the melt's degassed water content (C_{ld}) and hence the degassed magma's density (ρ_{md}) and viscosity (μ_{md}). The chamber-gas volume fraction influences the ascending density (ρ_{mc}), the amount of cooling due to decompression, and hence the degassed magma viscosity (μ_{md}). An additional variable is the magma chamber depth (H_c), which determines the chamber-gas pressure and density and hence the degree of decompression cooling. We calculated gas fluxes from conduits filled with degassing basaltic and dacitic magmas for a range of values for one variable, while holding the other variables constant. Results for basalt are shown in Fig. 4, for constant values of $\Delta C = 0.004$, $R = 5$ m, $C_c = 0.005$, $\phi_c = 0.3$, $H_c = 2$ km, $T_c = 1000\,^\circ$C, and three values of α (0, 0.02, and 0.04) in Fig. 4, and three values of H_c (2, 4, 8 km) in Fig. 4d. These values were chosen to be representative of Stromboli's magma system, and they yield water fluxes of 0–100 kg s^{-1}, of the correct order of magnitude (see below). Equivalent results for dacite are shown in Fig. 5, where the constant values used were representative of the Mount St. Helens magma system: $\Delta C = 0.023$, $R = 40$ m, $C_c = 0.046$, $\phi_c = 0.39$, $T_c = 910\,^\circ$C, $\alpha = 0$, 0.01, and 0.02, and $H_c = 4$, 7, and 10 km. These values yield water fluxes of 0–5000 kg s^{-1}, again covering the observed range (see below).

Basalt

Figure 4a illustrates that the degassing rate is proportional to the conduit radius to the fourth power. Figure 4b shows that the water flux increases approximately linearly with ΔC. Flux decreases with increased ϕ_c (Fig. 4c), because of the increase in viscosity, reduction in density contrast, and the reduced amount of melt available to release water. Figure 4d illustrates that for reasonable values of chamber-gas volume fraction, water flux is enhanced as α increases due to the lower density of the rising chamber magma. However, for high values of α (>0.05 for $H_c = 8$ km), and especially for deeper chambers, cooling of the ascending magma significantly increases the viscosity and reduces the water flux (see Appendix).

Application to Stromboli

Allard et al. (1994) reported a mean non-eruptive SO_2 flux of 9 ± 5 kg s^{-1} from Stromboli between 1980 and 1993, measured by COSPEC, and a mean H_2O:CO_2:SO_2 mass ratio in fumaroles of 7.9:7.3:1. This indicates a water flux of 70 ± 40 kg s^{-1} and a similar CO_2 flux (Allard et al. 1994). If we assume a chamber depth of 2 km, a chamber melt water content of 0.5 wt. %, and a crystal content of 30% (typical values for basalt; e.g., Giberti et al. 1992), then for the upper and lower bounds of the water flux (30 and 110 kg s^{-1}) and a $[H_2O]/[CO_2]$ ratio of 1.1, we can calculate a family of solutions for R and ΔC. The chamber-gas volume

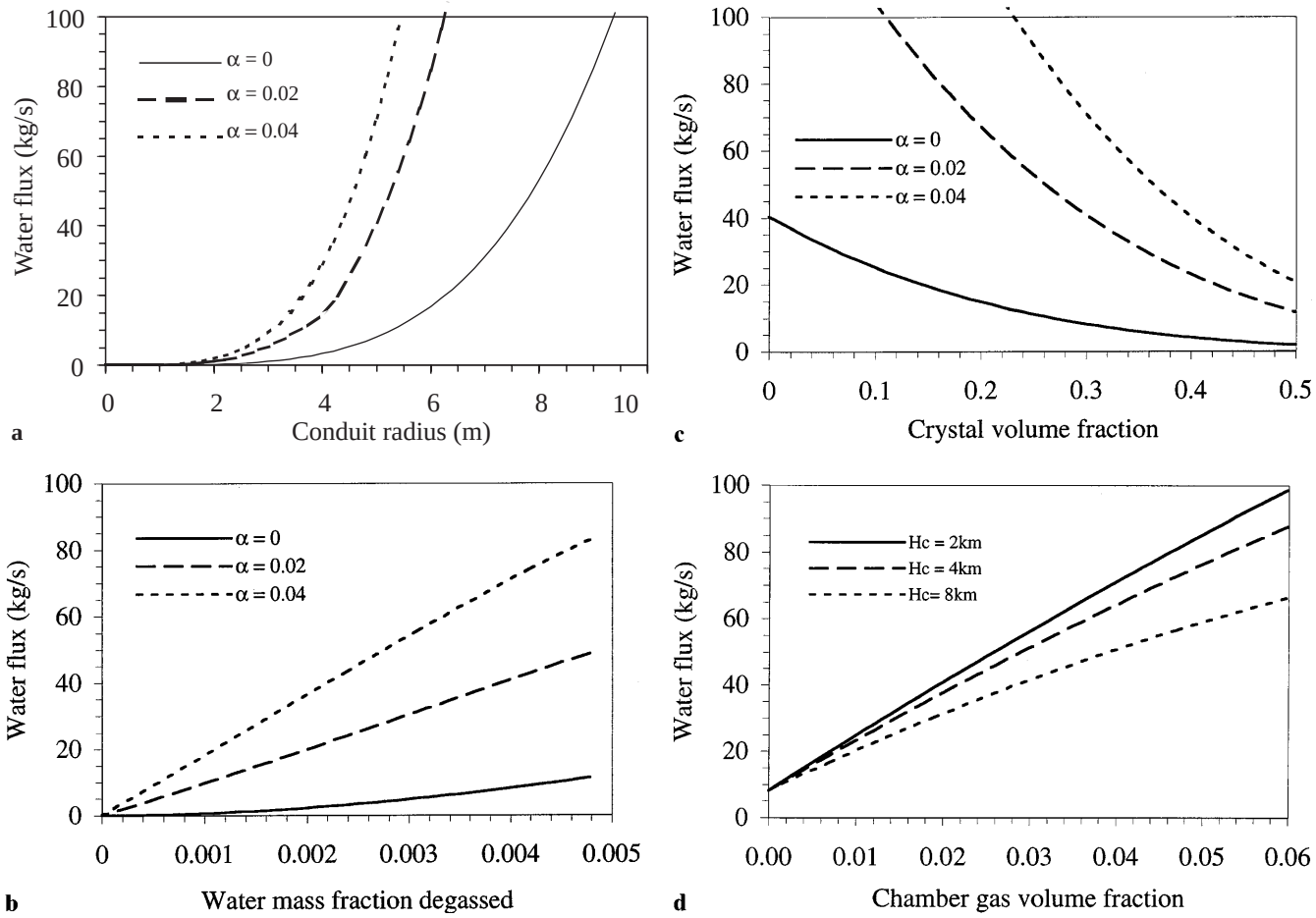

Fig. 4a–d Model results for basalt, showingthe variation of water mass flux ($\dot{m}_{H2O}$) with: **a** conduit radius (R); **b** water mass fraction degassed (ΔC); **c** crystal volume fraction (ϕ_c); and **d** gas volume fraction in the chamber (α). The fixed values used were R = 5 m, C_c = 0.005, ΔC = 0.004, ϕ_c = 0.3, T_c = 1000 °C, and H_c = 2 km

fraction is related approximately linearly to ΔC through Eq. 10, fixed by the values for $[H_2O]/[CO_2]$, H_c (and hence ρ_{CO2}), and ϕ_c. The solutions (Fig. 6) show that for reasonable amounts of water degassed from the Stromboli melt (20–100% water loss), the conduit radius falls in the range 4–10 m, and the magma chamber gas volume fraction is 1–4%. Almost complete water degassing seems likely at Stromboli, as the vents are essentially open to the atmosphere.

These model results seem reasonable in the light of surface observations of vents at Stromboli that indicate several conduits of a few meters radius, although it is not known if these coalesce or change size or shape with depth. In addition, a significant chamber-gas fraction has been inferred from previous modelling (Jaupart and Vergniolle 1989) in order to explain the observed periodic Strombolian activity.

Dacite

Results for a degassing dacite-filled conduit are shown in Fig. 5, using the 1980 Mount St. Helens composition (Rutherford et al. 1985). These show similar trends to the equivalent diagrams for basalt with the notable exception of Fig. 5b, the variation of gas flux with ΔC, which shows an optimum degassing amount for this system of ~25% of the available water. When a larger proportion of the dissolved water is lost from the melt, $\Delta\rho$ increases, but this effect is overshadowed by the higher viscosity of the drier degassed melt, so that gas fluxes decrease. The opposite is true when less than the optimum amount of water is lost – the decreasing amount of water exsolved and the lessening density contrast outweigh the effect of lower viscosity.

Application to Mount St. Helens, 1980

Casadevall et al. (1983) and McGee (1992) report SO_2 and CO_2 gas fluxes from Mount St. Helens following the May 1980 eruption. SO_2 fluxes peaked in July 1980 at a value of ~1500 t d^{-1}, or 17 kg s^{-1}. Fluxes have typical errors of ~30%. CO_2 fluxes were ~140 kg s^{-1} at the same time. Gerlach and Casadevall (1986) used gas measurements to model the evolution of the gas com-

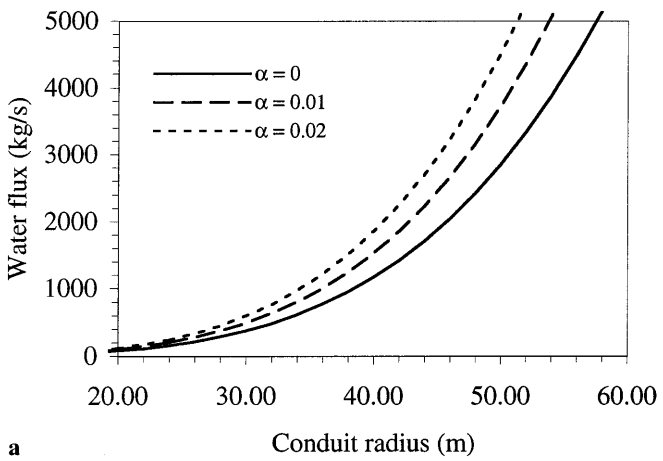

a

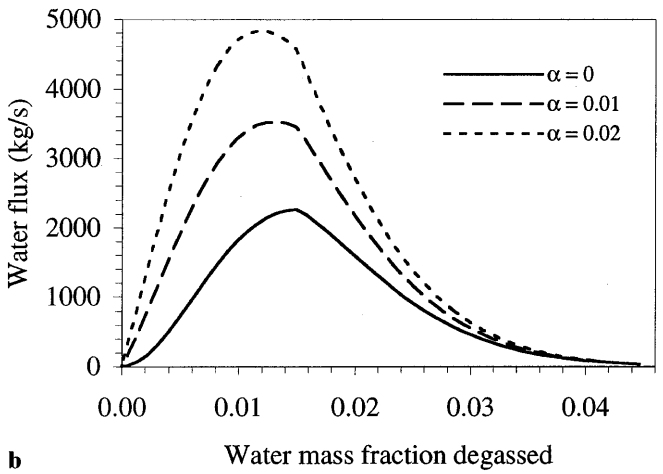

b

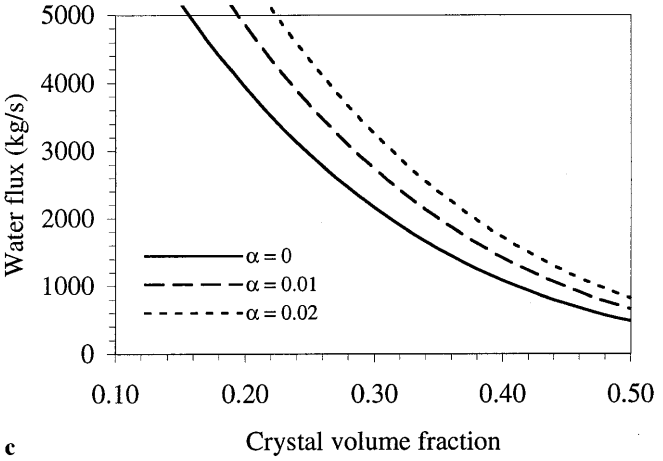

c

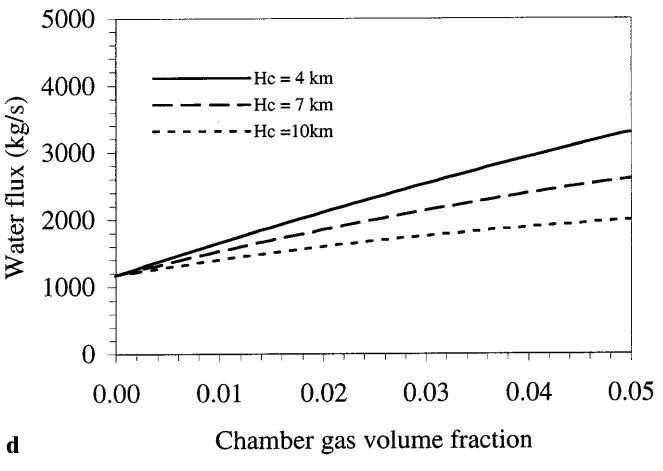

d

Fig. 5a–d Same as Fig. 4, but for dacite. The fixed values used were R = 40 m, $C_c = 0.046$, $\Delta C = 0.023$, $\phi_c = 0.39$, $T_c = 910\,°C$, and $H_c = 7$ km

position in the months following the eruption. They calculated a gas composition (assuming all H_2S is oxidized to SO_2 in the plume) with a H_2O:CO_2:SO_2 mass ratio of 50:12:1 for mid-June. Using these ratios to calculate a water flux yields values of ~400–1100 kg s^{-1}, with the lower value derived from the SO_2 flux. Gerlach and Casadevall (1986) also estimated that 20–40% of the H_2O in the gases was hydrothermal in origin at that time. Assuming a value of 30%, this suggests a magmatic water flux range of ~300–800 kg s^{-1} and that the magmatic H_2O:CO_2 mass ratio was 2.9. Assuming a 7 km deep chamber (Pallister et al. 1992), a chamber water content of 4.6 wt.%, and a crystal content of 39 vol.% (Rutherford et al. 1985), we can calculate a family of solutions for R and ΔC. Results (Fig. 7) show that for conduits of radius 40–60 m, the likely range suggested by Pallister et al. (1992), two degassing regimes are theoretically possible. The first involves relatively inefficient degassing, of only ~2–9 % of the available water, from a gas-poor chamber (~0.1–0.2%). The second involves much more efficient degassing, of ~60–90% of the available water, from a

Stromboli

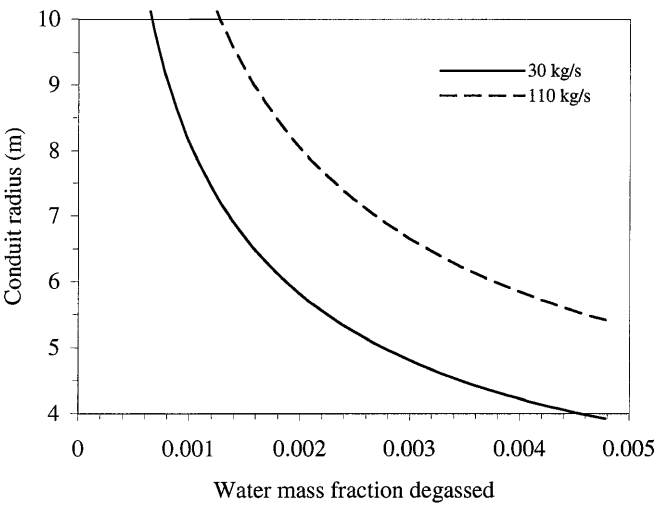

Fig. 6 Model results for Stromboli, assuming the following values: $C_c = 0.005$, $\phi_c = 0.3$, $T_c = 1000\,°C$, $H_c = 2$ km, $[H_2O]/[CO_2] = 1.1$, and $\dot{m}_{H2O} = 30$–110 kg s^{-1}. For reasonable values of ΔC (0.001–0.005; equivalent to 20–100% degassing), calculated conduit radii are ~4–10 m. From Eq. (10), $\alpha \approx 8\,\Delta C$ for the above values, and α falls in the range ~1–4%

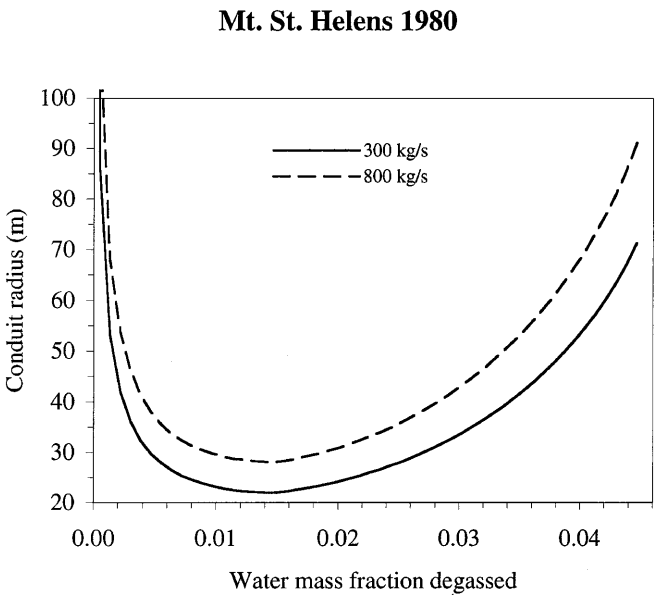

Fig. 7 Model results for Mount St. Helens in June 1980, assuming the following values: $C_c = 0.046$, $\phi_c = 0.39$, $T_c = 910\,°C$, $H_c = 7$ km, $[H_2O]/[CO_2] = 2.9$, and $\dot{m}_{H2O} = 300$–$800\ kg\ s^{-1}$. For reasonable values of the conduit radius (40–60 m; Pallister et al. 1992), two theoretical degassing regimes are identified, one with low values of ΔC (inefficient degassing) and the other at relatively high values of ΔC (efficient degassing). From Eq. (10), $\alpha \approx 0.6\ \Delta C$ for the above values, yielding $\alpha \approx 0.2\%$ in the first case, and $\alpha \approx 2\%$ in the second case

relatively gas-rich chamber ($\sim$2–3%). The narrowest viable conduit has a radius of 22–28 m, corresponding to the optimum degassing situation depicted in Fig. 5b.

Discussion of model assumptions

Gas-loss mechanism

We have assumed that convective overturn, rather than gas exsolution and escape, is the rate-limiting process for degassing. This assumption is more likely to hold for low-viscosity magmas, and the model is most applicable to persistently active basaltic systems. Application of the model to more viscous magmas is more uncertain, as the process of gas escape from such magmas remains poorly understood. However, the model returns reasonable values for the key parameters at Mount St. Helens, suggesting that it may be valid across a wide range of magma compositions.

We assume that all of the evolved and chamber-gas bubbles are lost during degassing, as the retention of even a small fraction of free gas will lower the density of the 'degassed' magma, causing a stable stratification in the conduit, inhibiting overturn. In addition to the gas-loss timescale, the timescale for the segregation of degassed melt and gas bubbles (e.g., Vergniolle and Jaupart 1986) may also be important. If gas loss or bubble segregation, rather than convection, is the rate-limiting process for degassing, then we might expect discontinuous magma convection to occur in the conduit, and the model would only give an upper limit for the gas emission rate.

Crystallization in the conduit

We have neglected changes in the crystal content of the magma during a convective cycle. This assumption is more reasonable for basaltic systems, where overturn rates are high. In the more slowly overturning, higher-viscosity systems, crystallization is more likely, but its impact on the model is likely to be relatively easily understood, inducing an increase in the degassed magma viscosity (Eq. 7), reducing the gas flux (Fig. 5c).

Conclusion

We have developed a model of convective overturn of dense degassed magma with buoyant volatile-rich magma in a conduit connected to a deep magma chamber. Laboratory modelling of the overturn of two fluids of different densities and viscosities in a narrow vertical pipe has shown that the style of overturn involves low-viscosity material (undegassed magma) rising up the centre of the conduit, with high-viscosity material (degassed magma) sinking along the walls (Fig. 2). These experiments define the correlation between flow rate and viscosity ratio reported in Fig. 3. Modelled gas fluxes increase as the conduit widens and the crystallinity decreases. Degassing rates from basaltic magmas increase with the amount of water degassed (ΔC), as this is directly related to the density difference ($\Delta\rho$) driving convection. In more silicic magmas, degassing rates increase, then decrease, with ΔC because the viscosity increase counteracts the increase in $\Delta\rho$. The model also incorporates the adiabatic cooling of deep CO_2-saturated magma as it rises to the degassing zone. Chambers containing more gas generally produce higher degassing rates, but cooling during ascent can cause the magma viscosity to increase sufficiently to reduce the gas flux from very deep and/or very gas-rich sources.

At Stromboli, the observed flux of $\sim 70\ kg\ s^{-1}$ magmatic water (and similar flux of CO_2) was modelled by a conduit of radius 4–10 m connecting a 2 km deep basalt chamber to the surface. Degassing releases 20–100% of the dissolved water in the chamber magma (assumed to be 0.5 wt.% H_2O, 30% crystals) and requires a chamber CO_2 gas volume fraction of 1–4 % in order to produce the observed fumarole composition. Degassing of $\sim 500\ kg\ s^{-1}$ magmatic water from Mount St. Helens in June 1980 was modelled with a conduit of radius 40–60 m connected to a 7 km deep dacite chamber, with 4.6 wt.% H_2O, and 39% crystals. Two theoretical degassing regimes fit the observed fluxes: (a) inefficient degassing of magma supplied from a relatively gas-poor

chamber; and (b) efficient degassing of magma supplied from a gas-rich chamber.

In summary, degassing-induced convection provides an efficient mechanism for gas release at shallow levels at the expense of the volatile content of a deep magma chamber.

Appendix: Cooling of the ascending magma due to gas decompression

The amount of cooling experienced by a decompressing magma parcel can be calculated, assuming the magma (melt plus gas mixture) expansion is adiabatic, the parcel has a constant mass fraction gas (i.e., there is no differential bubble rise or exsolution), and the gas and melt are in thermal equilibrium, from:

$$T_f = T_i \left(\frac{P_f}{P_i}\right)^{\left(\frac{\gamma-1}{\gamma}\right)} \quad \text{(A1)}$$

where T and P are temperature and pressure, the subscripts i and f refer to initial and final states, and γ is given by:

$$\gamma = \frac{(1-F)\,c_{v(melt)} + F\,c_{p(CO2)}}{(1-F)\,c_{v(melt)} + F\,c_{v(CO2)}} \quad \text{(A2)}$$

where F is the gas mass fraction, c_v is the specific heat capacity at constant volume, and c_p is the specific heat capacity at constant pressure. Values used are $c_{v(melt)} = 1000\ J\ kg^{-1}\ K^{-1}$, $c_{p(CO2)} = 1280\ J\ kg^{-1}\ K^{-1}$, and $c_{v(CO2)} = 1091\ J\ kg^{-1}\ K^{-1}$ (at 1200 K; Kaye and Laby 1986). Assuming that the density of any crystal fraction is the same as the melt density, then the gas mass fraction (F) is related to the gas volume fraction (α) by:

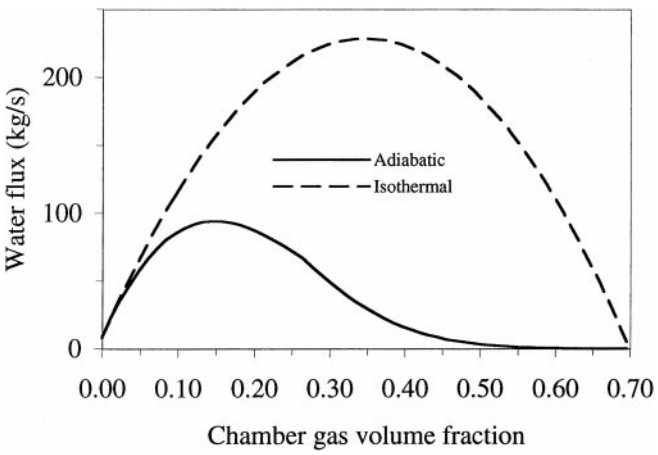

Fig. A1 Variation of water mass flux ($\dot{m}_{H2O}$) with gas volume fraction in the chamber (α), for the isothermal case (no decompression cooling) and the adiabatic case, for a basaltic system. The fixed values used were R = 5 m, $C_c = 0.005$, $\Delta C = 0.004$, $\phi_c = 0.3$, $H_c = 8$ km, and $T_c = 1000$ °C. The gas volume fraction extends to its theoretical maximum value of 70% (magma is all gas and crystals), although the maximum in practice is much lower

$$F = \frac{\alpha \rho_{CO2}}{(1-\alpha)\,\rho_{lc} + \alpha \rho_{CO2}} \quad \text{(A3)}$$

The density of CO_2 is calculated by assuming it is a perfect gas with a gas constant of 189 J kg^{-1} K^{-1}. The impact of including adiabatic cooling is shown in Fig. A1, which is an extension of Fig. 4d, for the case of an 8 km deep chamber. Figure A1 shows that the effect of adiabatic cooling is insignificant for values of $\alpha < \sim 5$ vol.% ($F < \sim 2$ wt.%) but then becomes increasingly important as the cooling induced by gas decompression increases the viscosity of the magma, causing a reduction in the water flux with increasing gas content, for $\alpha > \sim 15\%$ ($F > \sim 5$ wt.%).

The above calculations of cooling only include the chamber gas, assumed to be pure CO_2, and neglect cooling due to exsolution and expansion of water (Sahagian and Proussevitch 1996); hence, the amounts of cooling are minima.

Acknowledgements The paper was improved greatly by reviews from K. Cashman, J. Gardner, T. Koyaguchi, K. Kazahaya, and C. Carrigan.

References

Allard P, Carbonelle J, Métrich N, Loyer H, Zettwoog P (1994) Sulphur output and magma budget of Stromboli volcano. Nature 368:326–329

Allard P, Carbonelle J, Dajlevic D, Le Bronec J, Morel P, Robe MC, Maurenas JM, Faivre-Pierret R, Martin D, Saubroux JC, Zettwoog P (1991) Eruptive and diffuse emissions of CO_2 from Mount Etna. Nature 351:387–391

Casadevall T, Rose W, Gerlach T, Greenland LP, Ewert J, Wunderman R, Symonds R (1983) Gas emissions and the eruptions of Mount St. Helens through 1982. Science 221:1383–1385

Clift R, Grace JR, Weber ME (1978) Bubbles, drops and particles. Academic Press, London, pp 1–380

Eichelberger JC, Carrigan CR, Westrich HR, Price RH (1986) Non-explosive silicic volcanism. Nature 323:598–602

Francis PW, Oppenheimer C, Stevenson D (1993) Endogenous growth of persistently active volcanoes. Nature 366:554–557

Gerlach TM, Casadevall TJ (1986) Fumarole emissions at Mount St. Helens volcano, June 1980 to October 1981:degassing of a magma-hydrothermal system. J Volcanol Geotherm Res 28:141–160

Giberti G, Jaupart C, Sartoris G (1992) Steady-state operation of Stromboli Volcano, Italy: constraints on the feeding system. Bull Volcanol 54:535–541

Giggenbach WF (1987) Redox processes governing the chemistry of fumarolic gas discharges from White Island, New Zealand. Appl Geochem 2:143–161

Hurst AW, Bibby HM, Scott BJ, McGuinness MJ (1991) The heat source of Ruapehu crater lake; deductions from the energy and mass balances. J Volcanol Geotherm Res 46:1–11

Jaupart C, Allègre CJ (1991) Gas content, eruption rate and instabilities of eruption regime in silicic volcanoes. Earth Planet Sci Lett 102:413–429

Jaupart C, Vergniolle S (1989) The generation and collapse of a foam layer at the roof of a basaltic magma chamber. J Fluid Mech 203:347–380

Kaye GWC, Laby TH (1986) Tables of physical and chemical constants and some mathematical functions, 15th edn. Longman, London, pp 1–568

Kazahaya K, Shinohara H, Saito G (1994) Excessive degassing of Izu-Oshima Volcano: magma convection in a conduit. Bull Volcanol 56:207–216

Koyaguchi T, Blake S (1989) The dynamics of magma mixing in a rising magma batch. Bull Volcanol 52:127–137

Lange RL, Carmichael ISE (1990) Thermodynamic properties of silicate liquids with emphasis on density, thermal expansion and compressibility. In: Nicholls J, Russell JK (eds) Modern methods of igneous petrology: understanding magmatic processes. Rev Mineral 24:25–64

Lister JR, Kerr RC (1989) The effect of geometry on the gravitational instability of a buoyant region of viscous fluid. J Fluid Mech 202:577–594

McBirney AR, Murase T (1984) Rheological properties of magmas. Ann Rev Earth Planet Sci 12:337–357

McGee KA (1992) The structure, dynamics, and chemical composition of noneruptive plumes from Mount St. Helens, 1980–1988. J Volcanol Geotherm Res 51:269–282

Menyailov IA, Nikitina LP, Shapar VN, Pilipenko VP (1986) Temperature increase and chemical change of fumarolic gases at Momotombo Volcano, Nicaragua, in 1982–1985: Are these indicators of a possible eruption? J Geophys Res 91:12199–12214

Pallister JS, Hoblitt RP, Crandell DR, Mullineaux DR (1992) Mount St. Helens a decade after the 1980 eruptions: magmatic models, chemical cycles, and a revised hazards assessment. Bull Volcanol 54:126–146

Proussevitch AA, Sahagian DL, Kutolin VA (1993) Stability of foams in silicate melts. J Volcanol Geotherm Res 59:161–178

Rowe GL, Brantley SL, Fernandez M, Fernandez JF, Barquero J, Borgia A (1992) Fluid-volcano interaction in an active stratovolcano: the crater lake system of Poás Volcano, Costa Rica. J Volcanol Geotherm Res 49:23–51

Rutherford MJ, Sigurdsson H, Carey S, Davis A (1985) The May 18, 1980 eruption of Mount St. Helens. 1. Melt composition and experimental phase equilibria. J Geophys Res 90:2929–2947

Sahagian DL, Proussevitch AA (1996) Thermal effects of magma degassing. J Volcanol Geotherm Res 74:19–38

Shaw HR (1972) Viscosities of magmatic silicate liquids: an empirical method of prediction. Am J Sci 272:870–893

Stevenson DS (1992) Heat transfer in active volcanoes: models of crater lake systems. PhD thesis, Open University, UK, pp 1–235

Tait S, Jaupart C (1990) Physical processes in the evolution of magmas. In: Nicholls J, Russell JK (eds) Modern methods of igneous petrology: understanding magmatic processes. Rev Mineral 24:125–152

Vergniolle S, Jaupart C (1986) Separated two-phase flow and basaltic eruptions. J Geophys Res 91:12842–12860

Woods AW, Koyaguchi T (1993) Transitions between explosive and effusive eruptions of silicic magmas. Nature 370:641–644